Published in final edited form as:
J Neurophysiol. 1992 December ; 68(6): 2248–2259.

A Model of NMDA Receptor-Mediated Activity in Dendrites of Hippocampal CA1 Pyramidal Neurons

FERENC PONGRÁCZ, **NICHOLAS P. POOLOS**, **JEFFERY D. KOCSIS**, and **GORDON M. SHEPHERD**

Section of Neurobiology and Department of Neurology, Yale University School of Medicine, New Haven 06510; Neuroscience and Regeneration Research Center, Department of Veterans Affairs Medical Center, West Haven, Connecticut 06516; and Neuroscience Program, Stanford University, Stanford, California 94305

SUMMARY AND CONCLUSIONS

1. The role of synaptic activation of NMDA (*N*-methyl-D-aspartate) receptor-mediated conductances on CA1 hippocampal pyramidal cells in short-term excitability changes was studied with the use of a computational model. Model parameters were based on experimental recordings from dendrites and somata and previous hippocampal simulations. Representation of CA1 neurons included NMDA and non-NMDA excitatory dendritic synapses, dendritic and somatic inhibition, five intrinsic membrane conductances, and provision for activity-dependent intracellular and extracellular ion concentration changes.

2. The model simulated somatic and dendritic potentials recorded experimentally. The characteristic CA1 spike afterdepolarization was a consequence of the longitudinal spread of dendritic charge, reactivation of slow Ca^{2+}-dependent K^+ conductances, slow synaptic processes (NMDA-dependent depolarizing and γ-aminobutyric acid–mediated hyperpolarizing currents) and was sensitive to extracellular potassium accumulation. Calcium currents were found to be less important in generating the spike afterdepolarization.

3. Repetitive activity was influenced by the cumulative activation of the NMDA-mediated synaptic conductances, the frequency-dependent depression of inhibitory synaptic responses, and a shift in the potassium reversal potential. NMDA receptor activation produced a transient potentiation of the excitatory postsynaptic potential (EPSP). The frequency dependence of EPSP potentiation was similar to the experimental data, reaching a maximal value near 10 Hz.

4. Although the present model did not have compartments for dendritic spines, Ca^{2+} accumulation was simulated in a restricted space near the intracellular surface of the dendritic membrane. The simulations demonstrated that the Ca^{2+} component of the NMDA-operated synaptic current can be a significant factor in increasing the Ca^{2+} concentration at submembrane regions, even in the absence of Ca^{2+} spikes.

5. Elevation of the extracellular K^+ concentration enhanced the dendritic synaptic response during repetitive activity and led to an increase in intracellular Ca^{2+} levels. This increase in dendritic excitability was partly mediated by NMDA receptor-mediated conductances.

6. Blockade of Ca^{2+}-sensitive K^+ conductances in the dendrites increased the size of EPSPs leading to a facilitation of dendritic and somatic spike activity and increased $[Ca^{2+}]_i$. NMDA

Address for reprint requests: J. D. Kocsis, Neuroscience and Regeneration Research Center, Dept. of Veterans Affairs Medical Center, West Haven, CT 06516.

receptor-mediated conductances appeared as an amplifying component in this mechanism, activated by the relatively depolarized membrane potential.

7. The results suggest that dendritic NMDA receptors, by virtue of their voltage-dependency, can interact with a number of voltage-sensitive conductances to increase the dendritic excitatory response during periods of repetitive synaptic activation. These findings support experimental results that implicate NMDA receptor-mediated conductances in the short-term response plasticity of the CA1 hippocampal pyramidal neuron.

INTRODUCTION

N-methyl-D-aspartate (NMDA) receptors on the dendrites of hippocampal pyramidal neurons have a well-established role in the induction of long-term potentiation. During high-frequency, repetitive synaptic stimulation, NMDA receptor-mediated conductances become activated, allowing an influx of calcium into the postsynaptic membrane, which triggers a cascade of events leading to modification of synaptic excitability (reviewed by Nicoll et al. 1988). Because NMDA receptor-mediated conductances are relieved of a voltage-dependent block at depolarized membrane potentials, their activation during high-frequency stimulation is possibly a consequence of the summation of non-NMDA receptor-mediated excitatory postsynaptic potentials (EPSPs). Other studies, however, have shown activation of NMDA receptor-mediated conductances with as few as two synaptic stimuli at low frequencies or with a single stimulus under conditions of disinhibition, potassium channel blockade, or elevated extracellular potassium concentrations (Poolos and Kocsis 1990a,b; Wigstrom et al. 1985). These data suggest that NMDA receptor-mediated postsynaptic potentials may depend on the interaction of several postsynaptic conductances. One possibility is that the relatively slow kinetics of the NMDA-activated channel could be influenced by synaptic and intrinsic conductances, which hyperpolarize the membrane after each synaptic stimulus; a relative decrease in the effectiveness of these synapses might allow a sufficiently prolonged depolarization for NMDA receptor-mediated conductances to become fully activated. Unfortunately it is difficult to test rigourously such hypotheses with conventional recording methods in a hippocampal slice preparation.

To investigate interactions between NMDA receptor-mediated conductances and other dendritic conductances, we turned to numerical simulation of an idealized CA1 hippocampal pyramidal neuron. Previous numerical models have explored the properties of CA3 hippocampal neurons, both singly and in large networks, in part demonstrating the strong effect of the anatomic distribution of ionic conductances on the overall synaptic response of the cell (Traub and Llinas 1979; Traub et al. 1991). Other investigators have focussed on models of the dynamics of NMDA receptor-mediated conductances in isolated dendritic spines, which have shown the influence of NMDA receptor-mediated calcium influx on intracellular calcium levels (Gamble and Koch 1987; Holmes and Levy 1990). The present model seeks to bridge these two levels of analysis by representing a single, multicompartmental neuron with a nonhomogeneous distribution of known ionic conductances. This representation is novel in its incorporation of NMDA receptor-mediated conductances, together with γ-aminobutyric acid A ($GABA_A$) and $GABA_B$ receptor-mediated inhibitory conductances, five intrinsic membrane channel conductances, and a provision for activity-dependent changes in calcium and potassium concentrations. This model should enable investigation of hypotheses concerning the interactions between the several types of voltage-dependent channels present on hippocampal neuronal dendrites and their effects on NMDA receptor-mediated conductances, which are difficult to test under experimental conditions. With the present model, our goal was to observe how the complex kinetics of NMDA receptor-mediated conductances might interact with intrinsic and synaptic conductances to produce short-term changes in the excitability of CA1 neurons.

METHODS

Our general approach to modeling the CA1 hippocampal pyramidal cell was similar to that used by Traub and Llinas (1979) and Traub (1982). This modeling technique is based on modified Hodgkin-Huxley equations and the cable properties of idealized dendritic trees (Rall 1977). We represented the apical and basal trees of the CA1 cell by separate equivalent cylinders of five compartments each, with one compartment for the soma and one compartment for the axon initial segment (IS). The rest of the axon was lumped together in a large passive compartment that terminated by an infinite resistance. The small number of compartments helped us to carry out many simulations within a reasonable time period. The electrotonic length was chosen to be 0.8 λ for the apical dendritic cylinder and 0.6 λ for the basal dendritic cylinder, which are in the range observed by Turner and Schwartzkroin (1980). We used τ_m = 80 ms, giving C_m = 1 μF/cm^2 and R_m = 80,000 Ω-cm^2. With this R_m and R_i = 100 Ω-cm, our model had an R_{input} = 79 MΩ, which is somewhat lower than the range of recent patch-clamp data (Konnerth et al. 1990; Sah et al. 1990). Similar to the CA1 model of Traub and Llinas (1979), the R_m and C_m values of the IS were changed to decrease the reversal potential of the leak and to speed up the IS response (R_m = 1,000 Ω-cm^2, C_m = 0). The other part of the axon had a larger intracellular resistance (R_i = 166 Ω-cm) and smaller R_m value (R_m = 500 Ω-cm^2, C_m = 1 μF/cm^2). In contrast to earlier models of hippocampal pyramidal cells, we made the K^+ reversal (V_K) sensitive to the extracellular K^+ concentration. The positive shift in V_K, resulting from extracellular potassium accumulation, was found to be an important parameter in modifying the dendritic inhibitory potential, K^+-dependent outward currents, and consequently, the activation of NMDA receptor-mediated conductances. However, the resting depolarization of the CA1 neuron, which resulted from shifts in V_K remained less in the model than in the experiments (Poolos and Kocsis 1990a), which, according to the model equations, was a consequence of the small fraction of conductances conducting at rest in the model cell. Table 1 summarizes the geometric characteristics and the electrotonic lengths of the model cell under study.

The activation of ionic currents in the CA1 cells was influenced by three sets of equations as described below:

1. *Active conductances*. The well-known Hodgkin-Huxley equations for the active sodium and potassium currents were used

$$I_{NA} = \bar{g}_{Na} m^3 h (V - V_{Na}) \quad (1)$$

$$I_K = \bar{g}_K n^4 (V - V_K) \quad (2)$$

where $\bar{g}_{Na}$ and $\bar{g}_K$ are the peak conductance densities of the sodium and potassium channels, respectively; m, h, and n are the voltage-dependent state variables; V denotes the membrane potential relative to rest and V_{Na} = 115 mV and V_K = −15 mV are the reversal potentials. The model resting potential, according to our mathematical notation, was 0 mV and was assumed to correspond to −70 mV. The rate functions and the peak densities are listed in Tables 2 and 3, respectively. The fast sodium and potassium conductances had similar kinetics as proposed for CA3 cells (Traub 1982). The excitability of the IS was enhanced by choosing a higher peak density for g_{Na}. Fast spikes were evoked in the soma-IS complex and, in many cases, we considered a dendritic spike generator for the apical dendritic cylinder (Miller et al. 1985;Perkel and Perkel 1985;Pongrácz 1985;Shepherd and Brayton 1987).

The kinetics of the Ca^{2+} (g_{Ca}) and the Ca^{2+}-mediated K^+ ($g_{K(Ca)}$, $g_{C(Ca)}$) conductances were similar to those of Traub et al. (1991). The inactivation of the Ca^{2+} conductance was not dependent on the Ca^{2+} concentration; the fast inactivation was approximated

with a voltage-dependent exponential decay term for *V* above resting potential. This calcium component was of the high-voltage–activated type. Two components of the outward K^+ current were represented as calcium dependent. One of these, $g_{K(Ca)}$, followed slow time kinetics and contributed to a slow hyperpolarizing component after intensive spike activity. The activation of $g_{K(Ca)}$ depended on Ca^{2+} concentration but was not dependent on voltage and had no inactivation rate function. The other component, $g_{C(Ca)}$, was increased by intracellular calcium times a voltage-dependent term, with the activation time constant fast enough for the conductance to be partially activated during a single action potential.

In this model, a low level of partially activated $g_{K(Ca)}$ and $g_{C(Ca)}$ produced a small, constant outward current in steady state. This was carefully balanced in each compartment by calculating different leak batteries before starting the simulation. In the majority of simulations we used a low value for the peak density of the Ca^{2+} conductance ($\bar{g}_{Ca} = 0.2$ mS/cm^2) to prevent Ca^{2+} spikes (which were usually followed by depolarizing block). We used a constant value for the $\bar{g}_{K(Ca)}$ and $\bar{g}_{C(Ca)}$ (1 mS/cm^2), usually with a uniform distribution. The equations for these currents were

$$I_{Ca} = \bar{g}_{Ca} s^2 r (V - V_{Ca}) \tag{3}$$

$$I_{K(Ca)} = \bar{g}_{K(Ca)} q (V - V_K) \tag{4}$$

$$I_{C(Ca)} = \bar{g}_{C(Ca)} c \min [1, 0.0663([Ca^{2+}]_i / [Ca^{2+}]_{i,max})](V - V_K) \tag{5}$$

where *s* and *r* are the activation and inactivation state variables of the Ca^{2+} conductance, *q* is the activation state variable of the slow K^+ conductance ($g_{K(Ca)}$), and *c* is the voltage- and time-dependent state variable of the second, faster component of the Ca^{2+}-sensitive K^+ currents ($g_{C(Ca)}$). The relative calcium concentration ($[Ca^{2+}]_i/[Ca^{2+}]_{i,max}$) was used in the saturating term min [1, ($0.0663[Ca^{2+}]_i/[Ca^{2+}]_{i,max}$)] to have a unitless representation of intracellular Ca^{2+} accumulation. The scaling factor given by Traub et al. (1991) was changed accordingly. The maximal value of calcium concentration ($[Ca^{2+}]_{i,max}$) was computed at that membrane potential (in steady state) where the highest ratio of Ca^{2+} channels was opened ($s^2r = 0.25$ at $V = 10$ mV). The Ca^{2+} reversal was chosen to be 140 mV; *m*, *h*, *n*, *s*, *r*, *q*, and *c* all obey Hodgkin-Huxley-like equations of the type

$$dm/dt = \alpha_m (1 - m) - \beta_m m \tag{6}$$

2. *Compound synaptic conductance change*. The synaptic components of the model consisted of non-NMDA and NMDA receptor-mediated excitatory conductances and GABA receptor-mediated inhibitory conductances. The largest known group of the non-NMDA receptors corresponds to quisqualate receptors that are sensitive to agonists such as amino-3-hydroxy-methyl-4-isoxazdepropionic acid (AMPA; for review see Nicoll et al. 1990). The fast AMPA excitatory conductance carried Na^+ and K^+ currents, whereas the NMDA conductance conducted Ca^{2+} with a high permeability, in addition to Na^+ and K^+ (Ascher and Nowak 1988; Jahr and Stevens 1987; Mayer and Westbrook 1987a,b). The two inhibitory channels ($GABA_A$, $GABA_B$) were separated according to their ability to pass Cl^- and K^+ ions and their presumed somatic and dendritic localizations, respectively (Nicoll et al. 1990). The classic inhibitory receptor channel ($GABA_A$) has the ability to pass Cl^- ions and stabilizes the cell's resting potential and controls the spike threshold at the axon initial segment. $GABA_B$ receptor activation in hippocampal pyramidal cells' dendrites results in hyperpolarization due to an increase in membrane conductance to K^+ (Nicoll et al. 1990). NMDA, non-NMDA, and $GABA_B$ receptor-mediated conductances were

distributed into the apical five compartments of the dendritic cylinder, as shown in Fig. 1. Activation of the AMPA synaptic conductances was expressed as

$$g_{\mathrm{AMPA}}=\bar{g}_{\mathrm{AMPA}}\left(1-e^{-t/0.3}\right)e^{-t/3} \tag{7}$$

where t is in milliseconds. The NMDA receptor-mediated conductance was fitted with the biexponential function for fast and slow components given by Konnerth et al. (1990). The time constants of the fast (τ_{fast}) and slow (τ_{slow}) components were increased exponentially on depolarization

$$g_{\mathrm{NMDA}}=\bar{g}_{\mathrm{NMDA}}(1.58e^{-t/\tau_{\mathrm{fast}}}-e^{-t/\tau_{\mathrm{slow}}})/(1+0.66e^{-0.07(V-60)}) \tag{8}$$

where V is in millivolts, and

$$\tau_{\mathrm{fast}}=(46\ \mathrm{ms})\,e^{V/83}$$

and

$$\tau_{\mathrm{slow}}=(235\ \mathrm{ms})\,e^{V/121} \tag{9}$$

Equation 8 includes a voltage- and mangnesium-dependent Boltzmann in the form reported by Jahr and Stevens (1990b) and used by Traub et al. (1991). Similar voltage dependence of the NMDA receptor-mediated component can be determined by fitting a curve to the voltage-clamp data of Mayer and Westbrook (1987b: Fig. 4). In Eqs. 7 and 8, $\bar{g}_{\mathrm{AMPA}}$ and $\bar{g}_{\mathrm{NMDA}}$ are mediated by the non-NMDA and NMDA receptors. V represents the membrane potential relative to rest. The reversal potentials for the current components were set to 70 mV relative to rest (AMPA component) and 75 mV (NMDA receptor-mediated component). The inhibitory mechanism acting in the input compartment was assumed to be a $GABA_B$-mediated inhibition with rapid onset and slow decay. This experimentally identified large conductance ($g_{\mathrm{GABA,B}}$) was activated at the same time as the excitatory components and inactivated slowly to influence the interpulse intervals without large overlap at 10 Hz. The experimental data on paired pulse depression of $GABA_B$-mediated inhibition (Davies et al. 1990; McCarren and Alger 1985) led us to decrease $g_{\mathrm{GABA,B}}$ from 100% to 25% with the change of the interstimulus intervals of between 10 ms and 1 s (the maximum depression of $g_{\mathrm{GABA,B}}$ was at interval of 100 ms: see Fig. 6 in Davies et al. 1990)

$$g_{\mathrm{GABA,B}}=\bar{g}_{\mathrm{GABA,B}}S_{\mathrm{depr}}\left(1-e^{-t/2}\right)e^{-t/100} \tag{10}$$

Where

$$S_{\mathrm{depr}}=0.25-0.75[\log(T)+1] \quad \text{if } 10\ \mathrm{ms}<T\le 100\ \mathrm{ms}$$
$$S_{\mathrm{depr}}=0.25+0.75[\log(T)+1] \quad \text{if } 100\ \mathrm{ms}<T<1\mathrm{s}$$

else

$$S_{\mathrm{depr}}=1.0 \tag{11}$$

S_{depr} represents the decrease of the $g_{\mathrm{GABA,B}}$ as a function of the length of interstimulus interval (T) in a train of synaptic excitation. A decreased K^+ reversal can also reduce the dendritic inhibition in CA1 cells (McCarren and Alger 1985) implying that the K^+ ions would be the main charge carriers. By comparing the results of several simulations to experimental data, we found a good agreement if the ratios of the conductances were

$$\bar{g}_{\mathrm{NMDA}}:\bar{g}_{\mathrm{AMPA}}:\bar{g}_{\mathrm{GABA,B}}=8\ \mathrm{nS}:160\ \mathrm{nS}:40\ \mathrm{nS} \tag{12}$$

In some cases $\bar{g}_{\mathrm{AMPA}}$ had different values depending on the rate of stimulation.

We have included in the soma compartment an effective amount of classic $GABA_A$ "shunting inhibition" mediated by Cl^- ions (Allen et al. 1977; Davies et al. 1990; Nicoll et al. 1990). The onset of the underlying inhibitory conductance ($g_{GABA,A}$) was delayed by 2 ms from the onset of the dendritic synaptic events

$$g_{GABA,A} = \bar{g}_{GABA,A}(1 - e^{-t/2})e^{-t/100} \quad (13)$$

which yields a time course similar to its dendritic counterpart. The value given to $\bar{g}_{GABA,A}$ (20 nS) was enough to decrease the spike-afterdepolarization and increase the spike threshold at the soma. The reversal of this inhibitory component was set at the resting potential (0 mV), approximating the equilibrium potential of Cl^-. This reversal did not depend on the change in extracellular K^+ concentration ($[K^+]_o$), and consequently, the current flowing through $g_{GABA,A}$ was less sensitive to the preceding synaptic activity than the current through $g_{GAHA,B}$.

In summary, the synaptic currents included in the CA1 model neuron were

$$I_{Syn,dend} = I_{AMPA} + I_{NMDA} + I_{GABA,B} = g_{AMPA}(V - V_{AMPA}) + g_{NMDA}(V - V_{NMDA}) + g_{GABA,B}(V - V_K) \quad (14)$$

$$I_{Syn,soma} = I_{GABA,A} = g_{GABA,A}(V - V_{Cl}) \quad (15)$$

where $I_{Syn,dend}$ and $I_{Syn,soma}$ represent the compound synaptic current in dendrites aid cell body, respectively, and V_{AMPA}, V_{NMDA}, V_K and V_{Cl} are the reversal potentials.

It is well known that the NMDA receptor-mediated conductance has a high permeability to Ca^{2+} (Ascher and Nowak 1988; Jahr and Stevens 1987; Mayer and Westbrook 1987a,b). This Ca^{2+} current and its contribution to intracellular Ca^{2+} accumulation has been incorporated into the model. The NMDA receptor-mediated synaptic current consisted of Ca^{2+} ($g_{NMDA,Ca}$) and nonspecific ($g_{NMDA,\Sigma}$) components. The reversal potentials of the currents through these conductances were represented by V_{Ca} and $V_{NMDA,\Sigma}$

$$g_{NMDA}(V - V_{NMDA}) = g_{NMDA,Ca}(V - V_{Ca}) + g_{NMDA,\Sigma}\left(V - V_{NMDA,\Sigma}\right) \quad (16)$$

Where

$$g_{NMDA} = g_{NMDA,Ca} + g_{NMDA,\Sigma}$$

These equations can be solved to find and the ratios $g_{NMDA,Ca}/g_{NMDA}$ and $g_{NMDA,\Sigma}/g_{NMDA}$ and the unknown reversal $V_{NMDA,\Sigma}$. The experimental data suggested a conductance ratio $g_{NMDA,Ca}/g_{NMDA} = 0.11$ (Fig. 12 of Mayer and Westbrook 1987a). Using this result and the known values of equilibrium potentials, we calculated the appropriate value of $V_{NMDA,\Sigma}$ (61.3 mV, relative to rest).

Table 3 shows the range of the peak synaptic conductances used in the simulations.

3. *Internal calcium and external potassium concentrations.* Simplified models of ionic concentration changes were constructed by approximating the complex effects of fluxes, ionic pumps, diffusion, and buffers with a lumped parameter describing the loss of ions from a restricted space (Traub and Llinas 1977). Equations for estimating a change of the relative intracellular Ca^{2+} concentration ($[Ca^{2+}]_i/[Ca^{2+}]_{i,max}$) and the shift (from the resting value of 3 mM) in $[K^+]_o$ are given as

$$d([Ca^{2+}]_i/[Ca^{2+}]_{i,max})/dt = 0.059\ mM^{-1}(c_{Ca}/Ad_{Ca})(I_{Ca} + I_{NMDA,Ca}) - \beta_{Ca}([Ca^{2+}]_i/[Ca^{2+}]_{i,max}) \quad (17)$$

$$d[K^+]_o/dt = (c_K/Ad_K)(I_K + I_{K(Ca)} + I_{C(Ca)} + I_{GABA,B}) - \beta_K[K^+]_o \quad (18)$$

In Eqs. 17 and 18 particular current components can be zero depending on dendritic or somatic location. $I_{NMDA,Ca}$ represents the Ca^{2+} component mediated by NMDA receptors. The $[Ca^{2+}]_i/[Ca^{2+}]_{i,max}$ values were computed for the intracellular volume (shell) under the surface A to depth d_{Ca}(=2 Å), and the $[K^+]_o$ values (in mM) were estimated for the extracellular volume of thickness d_K(=200 Å: see Gardner-Medwin 1983 for derivation of the parameters of $[K^+]_o$ fluxes). An explanation for the appropriate selection of dimensions of intracellular Ca^{2+} shell can be found in Traub and Llinas (1979) and Traub (1982). β_{Ca} = 0.1/ms and β_K = 0.2/ms (dendrite) and 0.1/ms (soma) were used to represent the time decays of the concentrations. c_{Ca} = 5,200 mM/10^6 C and c_K = 10,400 mM/10^6 C were the conversion constants. In Fig. 1, the external shell around the compartment model represents the extracellular volume for K^+. The activations of two potassium conductances ($g_{K(Ca)}$, $g_{C(Ca)}$) were controlled by $[Ca^{2+}]_i/[Ca^{2+}]_{i,max}$ $[K^+]_o$ was used to calculate the activity-dependent shift in the potassium reversal at each compartment according to the Nernst equation. The large peaks of $[K^+]_o$ transients following action potentials were decreased in some cases by multiplying the $[K^+]_o$ by an exponential term ($e^{-[K^+]_o/5mM}$), which represented an enhanced removal of $[K^+]_o$ from the extracellular shell.

Consideration was given to comparing the "lumped" model of $[Ca^{2+}]_i$ to more detailed models that include spines (Gamble and Koch 1987; Holmes and Levy 1990; Wickens 1988). This issue is especially important in CA1 cells where the NMDA receptor-mediated synaptic current can be a significant factor in increasing the Ca^{2+} concentration in the spine head. The present model produces a relatively simple link between the lumped (cooperative) Ca^{2+} activity in the dendrites and the experimentally recorded physiological activity of the cell. Quantitative comparison can be made by calculating an average Ca^{2+} content in proximal spine necks, assuming that the $[Ca^{2+}]_i$ in the submembranous region predicted by the present model resulted from a diffusion at spine contacts (choosing a small dendritic shaft with realistic spine density). However, the comparison is complicated by the large, ill-determined ratio between the surface area of dendrites and the contact area of the attached spines. The present simulations allowed qualitative conclusions about the sources of the intracellular calcium accumulation and its effects on other calcium-dependent conductances.

Our computational technique utilized a general purpose circuit simulator program called SABER (Analogy Inc.), which is well suited for studying highly complex, nonlinear compartment systems (Carnevale et al. 1988).

RESULTS

Spread of soma-dendritic potentials in the presence of NMDA receptor-mediated conductance and potassium accumulation

Soma-dendritic potentials generated in response to a synaptic input are shown in Fig. 1 next to a schematic of the compartmental model. These responses closely simulate experimental intradendritic recordings (Poolos and Kocsis 1990b;Wong et al. 1979). The central compartment of the apical cylinder contained fast Na^+ and K^+ conductances and was able to generate action potentials. A small peak on the rising phase of the dendritic EPSP resulted from the activation of a spike generator in the nearby dendritic region. Figure 1 further demonstrates that the spike initiated in dendritic membrane invades a large portion of the apical dendrite, adding depolarization to that of the dendritically generated EPSPs.

The ionic conductances underlying the somatic and dendritic potentials are summarized in Fig. 2. The conductances showed large differences in their amplitudes and time courses. The

conventional g_{Na}, g_K, and g_{Ca} in the cell body had fast inactivation and therefore did not contribute to the spike-afterdepolarization (*A* and *C*). This afterdepolarization appears to be the result of longitudinal current spread from dendritic EPSP activity, which is opposed by slow repolarizing currents ($I_{C(Ca)}$, $I_{K(Ca)}$) and is not a reflection of somatic I_{Ca} as has been suggested for the CA3 hippocampal pyramidal cells (Traub and Llinas 1979). The g_{Ca}, $g_{C(Ca)}$, and $g_{K(Ca)}$ in the soma (*E*) remained at much lower levels than in the dendrites (*F*) despite the same conductance densities ($\bar{g}_{Ca}$, = 0.2 mS/cm^2 and $\bar{g}_{K(Ca)} = \bar{g}_{C(Ca)}$ = 1 mS/cm^2). The larger activation of dendritic g_{Ca} was a consequence of the prolonged dendritic potential (*B*), whereas the increase in $g_{K(Ca)}$ and $g_{C(Ca)}$ partially resulted from the NMDA receptor-mediated Ca^{2+} influx (*I*). The time course of Cl^--mediated inhibition ($g_{GABA,A}$) is shown in Fig. 2*G*, whereas the relationship of non-NMDA (g_{AMPA}), NMDA (g_{NMDA}) and K^+-mediated inhibitory conductances ($g_{GABA,B}$) are shown in Fig. 2*H*. In agreement with experimental observations (Collingridge et al. 1988;Poolos and Kocsis 1990a), the increase in g_{NMDA} was minimal during a single non-NMDA-mediated EPSP. Figure 2*I* compares the total NMDA receptor-mediated synaptic current to the Ca^{2+} component. Note that with conservative estimates of the calcium permeability of the NMDA receptor-mediated conductance, a large portion of the inward current is carried by Ca^{2+}.

Cumulative effect of activation of NMDA receptor-mediated conductances during repetitive activity

The subthreshold responses of the model neuron to repetitive synaptic stimulation showed short-term changes similar to those reported in experimental studies (Collingridge et al. 1988; Herron et al. 1986; Poolos and Kocsis 1990a,b). In Fig. 3, the dendritic and somatic responses elicited by repetitive (10 Hz) synaptic inputs in the model were compared in the presence (——) and absence (– – –) of NMDA receptor-mediated synaptic conductance ($\bar{g}_{NMDA}$ = 4 × 2 nS and 0). Experimental data indicate that the second EPSP of a train at the frequencies used here shows a step increase in amplitude that is independent of NMDA receptor-mediated events (Poolos and Kocsis 1990a). This was incorporated into the model by decreasing peak excitatory conductances of the first EPSP of the train by 20%. [The mechanism for this phenomenon may be related to a presynaptic facilitation with increased transmitter release; for review see Zucker (1989).] As can be seen in the superimposed traces, NMDA receptor-mediated conductances were activated during the stimulus train, inducing an increase in the amplitude of the EPSP and prolonged its falling phase. These changes reached a maximal level at the 5th or 6th pulse in a train and remained constant thereafter (Fig. 3, *A* and *B*). A spike generator was added to the central dendritic compartment of the apical cylinder (Fig. 3 *B*).

In contrast to the cumulative increase in I_{NMDA}, no similar tendency was found in the time course of the non-NMDA receptor-mediated synaptic current (Fig. 4*A*). However, the dendritic IPSP mediated by $g_{GABA,B}$ receptors was accompanied by a small frequency-dependent decrease in the amplitude of $I_{GABA,B}$ due to a transient decrease in V_K. This change in the dendritic inhibition was coincident with the maximal depression of $I_{GABA,B}$ during repetitive synaptic activity of 10 Hz (Fig. 4*A*). Figure 4, *B* and *C*, shows the dendritic potentials during the activation and blockade of g_{NMDA}, when the dendritic cylinder did not (*B*) or did (*C*) possess a spike generator. In both cases the activation of NMDA receptor-mediated conductance did not affect the EPSP to a single stimulus (*top traces*, Fig. 4*B*, and *C*), but did affect the subsequent EPSPs in the train.

To quantify the increases in both EPSP amplitude and duration, which occurred during short-term potentiation, we chose to measure the area bounded by the EPSP wave-form between EPSP onset and decay to resting potential before the afterhyperpolarization. The frequency dependence of the short-term potentiation was studied by comparing the area under the second

EPSP to a control value (at a frequency of 1 Hz) during a train of synaptic inputs delivered over a frequency range of 1–100 Hz (Fig. 5). We compared the EPSP potentiation in the presence and absence of NMDA receptor-mediated conductances for the cases of a subthreshold response (Fig. 5*A*) and activation of dendritic and somatic spike generators (Fig. 5*B*). In the absence of spike activity, the maximal g_{NMDA}-induced increase in potentiation of the postsynaptic response remained smaller than during the activation of the spike generators. The maximal value at 10 Hz appears to be related to the frequency-dependent depression of the inhibitory conductance $g_{GABA,B}$. The prediction of the model is in good correlation with experimental data (*A*, dotted diagram). Although the activation of NMDA receptor-mediated conductances does not significantly change the shape of the frequency dependence of the EPSP potentiation, it does amplify the size of the EPSP through a range of stimulus frequencies.

Intracellular Ca^{2+} accumulation evoked by NMDA receptor-mediated Ca^{2+} current

Changes in intracellular Ca^{2+} concentration during synaptic activity were calculated for a dendritic compartment containing NMDA receptor-mediated synaptic conductances according to Eq 17, and the results are shown in Fig. 6. As indicated previously from comparing the time courses of the conductances, the Ca^{2+} influx resulting from the NMDA receptor-mediated synaptic current was dominant during subthreshold activity in dendrites. The change of relative Ca^{2+} concentrations in a shell beneath the membrane was calculated without (*A* and *B*) and with (*C* and *D*) a dendritic spike generator. Three components of the ionic conductances were always present in a uniform distribution: $\bar{g}_{Ca} = 0.2$ mS/cm^2, $\bar{g}_{K(Ca)} = 1$ mS/cm^2, and $\bar{g}_{C(Ca)} = 1$ mS/cm^2. The Ca^{2+} level resulting from repetitive synaptic stimulation at 10 Hz was much higher during the activation of g_{NMDA}. The addition of dendritic spike generators decreased the relative contribution of g_{NMDA} to transient increases in $[Ca^{2+}]_i$, presumably by supplying additional dendritic depolarization that activated intrinsic g_{Ca}. The model predictions on the ratio of the g_{NMDA}-induced and g_{ca}-lnduced $[Ca^{2+}]_i$ accumulations with dendritic spike generators are in a good correlation with the results of the recent microfluorometric measurements (Regehr and Tank 1990). The cumulative effects of the g_{NMDA} on the dendritic potentials and Ca^{2+} accumulations are shown in *B* and *D* by shifting the baselines and onsets of the first and fifth transients to the same position. Without a spike-generating compartment in the apical cylinder the cumulative effect of the g_{NMDA} was much larger on the intracellular Ca^{2+} than on the dendritic EPSP (*B*). This difference decreased if one compartment of the apical cylinder was able to generate action potentials (*D*). In this case, the excitability increase mediated by the slow activation of the g_{NMDA} led to an increase in dendritic bursting.

Excitability changes due to $[K^+]_o$ increases and blockade of $g_{C(Ca)}$ and $g_{K(Ca)}$

In earlier electrophysiological studies (Poolos and Kocsis 1990a,b) it was shown that an increase in $[K^+]_o$ or a partial block of K^+ channels leads to an enhancement of dendritic potentials that is partly mediated by NMDA receptors. We investigated the cooperative effects of these parameters in the model neuron. Simulations were performed by choosing different initial values for $[K^+]_o$ in Eq. 18. Figure 7 summarizes the consequences of an elevated $[K^+]_o$ in comparison to the control $[K^+]_o$ (3 mM). Uniform distributions of soma-dendritic g_{Ca}, $g_{K(Ca)}$ and $g_{C(Ca)}$ were assumed with the previously defined values ($\bar{g}_{Ca} = 0.2$ mS/cm^2, $\bar{g}_{K(Ca)} = \bar{g}_{C(Ca)} = 1$ mS/cm^2). Because of the similarity with the experimental curves, we added a spike generation site in one compartment of the apical cylinder ($\bar{g}_{Na} = \bar{g}_{K} = 10$ mS/cm^2), which produced multiple peaks on the dendritic EPSPs.

As shown in Fig. 7*C*, elevated $[K^+]_o$ (5 mM) enhanced dendritic spike activity during repetitive stimulation, partly owing to a prolonged activation of NMDA receptor-mediated currents. Leaving the extracellular K^+ concentration high but blocking g_{NMDA} (Fig. 7*D*) suppressed dendritic spike generation and decreased the size of the successive synaptic responses. The depolarizing shift (ΔV) in resting potential as a function of $[K^+]_o$ remained less in the model

than in the experiments. No significant differences have been found in the somatic and dendritic ΔV values, consistent with experimental results. A larger shift in the initial $[K^+]_o$ (>7 mM) in the model led abruptly to a depolarizing block and a massive influx of Ca^{2+} through the dendritic Ca^{2+} conductance. This effect is present at this level of $[K^+]_o$ in the experimental results (Poolos and Kocsis 1990a).

In previous experiments it was found that low concentrations of a K^+ channel blocker [tetraethylammonium (TEA)] caused a substantial increase in amplitude and slowed repolarization of soma-dendritic potentials. It was suggested that TEA at these concentrations (1–2 mM) has its blocking effect on particular K^+ conductances activated predominantly in dendrites. These conductances appear to be Ca^{2+}-sensitive K^+ conductances [$g_{K(Ca)}$, $g_{C(Ca)}$). In the CA1 model, we compared the dendritic potentials and the Ca^{2+} concentration changes in the presence and absence of Ca^{2+}-sensitive K^+ conductances (Fig. 8). The response to a train of stimuli at 10 Hz showed a small amount of EPSP potentiation after blockade of $g_{K(Ca)}$ and $g_{C(Ca)}$ (*A* and *B*), which also contributed to an increase in the intracellular Ca^{2+} concentration (*C* and *D*). Figure 8, *E* and *F*, demonstrates that some of the excitability increase during the train of stimuli resulted from the activation of NMDA-mediated conductances acting cooperatively with the blockade of $g_{K(Ca)}$ and $g_{C(Ca)}$. The excitability changes seen with blockade of calcium-activated potassium conductances were smaller than noted experimentally (Poolos and Kocsis 1990a); it is possible that this was an artifact of a somewhat simplified model of calcium dynamics.

DISCUSSION

Activation of NMDA receptor-mediated conductances by repetitive stimulation

The model reproduces two key features of the dendritic response to repetitive synaptic stimulation, namely weak activation of NMDA receptor-mediated conductances with single synaptic stimuli and increasing activation with increasing number and intensity of stimuli. This effect is a consequence of the voltage dependence of the NMDA receptors and the different time courses of NMDA and non-NMDA receptor-mediated synaptic conductances. With a single stimulus, the synaptic voltage change mediated by non-NMDA receptors has peaked before the slowly activating NMDA receptor-linked conductance has reached its peak. At this point, the dendritic inhibitory conductances have also been activated, driving the membrane potential to a more hyperpolarized level. Although NMDA-mediated conductances are substantially blocked near resting potential, I_{NMDA} remains small during a single EPSP even though NMDA receptor-mediated conductances are in fact activated. The relative timing between the passive decay of the EPSPs and the peak value of g_{NMDA} is an important parameter that is determined by the electrotonic properties of the cell.

When multiple synaptic stimuli are delivered at frequencies of $\geq$ 5 Hz the long decay (Eq.9) of previously activated NMDA-mediated conductances allows a substantial increase in I_{NMDA} during the second and subsequent EPSPs in a train. For stimulation at 10 Hz, while the first EPSP produces only a small peak I_{NMDA}, the second EPSP arrives 100 ms later when I_{NMDA} is near zero but g_{NMDA} from the first stimulus has decayed to only 50–60% of its peak value. Because NMDA receptor-mediated conductances remain substantially activated (but blocked in a voltage-dependent manner) from the previous stimulus, significant I_{NMDA} can develop during the depolarization generated by the non-NMDA receptor-mediated EPSP.

With successive stimuli, summation of activated NMDA receptor-mediated conductances occurs and leads to further increases in I_{NMDA}. Note that the non-NMDA receptor-mediated conductance shows no change with repetitive stimulation because its channel kinetics are much faster than the stimulation rate shown here. The addition of the dynamic I_{NMDA} to the unvarying currents mediated by the non-NMDA receptors produces a composite EPSP that manifests a

degree of short-term potentiation. The maximal level of EPSP potentiation depends on the duration of the interstimulus interval that modifies the level of successive inhibition. The postsynaptic responses of actual CA1 pyramidal cells continue to show a lesser amount of potentiation when NMDA receptors are blocked (Poolos and Kocsis 1990a), representing other mechanisms of plasticity localized at non-NMDA glutaminergic synapses, GABAergic synapses, or other sites.

The EPSP potentiation at different stimulation frequencies has shown similar characteristics in the model and the experiments (Fig. 5). In our model the NMDA receptor-mediated conductance can induce low-frequency potentiation, which supports the evidence that processes dominating short- and long-term potentiations are located postsynaptically (Larson and Lynch 1986;Lynch et al. 1983;Wigstrom and Gustafsson 1984) but does not contradict recent data on the presynaptic contribution to long-term potentiation (Bekkers and Stevens 1990;Malinow and Tsien 1990). The model suggests that patches of active dendritic (as well as somatic) membrane impart a more strongly nonlinear postsynaptic response, mediating significant increases in postsynaptic activity in response to repetitive synaptic stimulation within a narrow range of frequencies. The experimental data and the model support the view that the excitability increase can lead to an enhancement of dendritic spikes, perhaps in a functionally important way.

Role of changes of $[K^+]_o$ and Ca^{2+}-sensitive K^+ conductances in dendritic excitability

The effect of increased $[K^+]_o$ on the excitability of hippocampal pyramidal cells has been studied in some depth (Poolos and Kocsis 1990a; Rutecki et al. 1985; Traynelis and Dingledine 1988), largely because of the correlation between epileptogenic seizures and elevated $[K^+]_o$ and the ability of the hippocampus to serve as an epileptogenic focus in temporal lobe epilepsy. In a previous paper (Poolos and Kocsis 1990a), increases in $[K^+]_o$ were found to potentiate the NMDA receptor-mediated component of the CA1 pyramidal cell dendritic EPSP. The present simulations reproduce this effect, showing increases in I_{NMDA} with elevation of $[K^+]_o \leq 5$–6 mM. However, the simplified structure of the model restricts the possible mechanisms underlying the effect of $[K^+]_o$ on NMDA receptor-mediated neurotransmission. For example, the magnitude of the synaptic conductance activated by each stimulus is unaffected by $[K^+]_o$ at the presynaptic terminal; i.e., there are no “presynaptic” effects, although such effects are known to occur (Kocsis et al. 1983; Poolos et al. 1987).

Although the effect of increased $[K^+]_o$ on resting potential is mitigated by membrane conductances to chloride and sodium, increased $[K^+]_o$ will have a more pronounced effect on intrinsic potassium conductances, which in this model include an inhibitory conductance ($g_{GABA,B}$) and Ca^{2+}-sensitive potassium conductances $g_{K(Ca)}$, $g_{C(Ca)}$. By lessening the driving force across these conductances, increased $[K^+]_o$ effectively delays the repolarization of the EPSP, which favors the slower activation kinetics of the NMDA receptor-mediated conductance, thus increasing I_{NMDA} during the EPSP. A similar phenomenon could be seen with blockade of $g_{K(Ca)}$ and $g_{C(Ca)}$ (Fig. 8), which produced an increase in the NMDA receptor-mediated current. Similarly, decreasing dendritic $g_{GABA,B}$ substantially increases I_{NMDA}; however, in these experiments we were unable to distinguish which of the potassium conductances had the greatest influence on the NMDA receptor activation. Reductions in repolarizing current through Ca^{2+}-activated potassium channels, whether through partial blockade or decreased driving force, led to increases in dendritic $[Ca^{2+}]_i$. This is consistent with the postulated function of Ca^{2+}-activated potassium conductances as limiting Ca^{2+} influx through voltage-sensitive channels; interestingly, in this model the elevations in dendritic Ca^{2+} influx were largely mediated by NMDA-linked conductances and not by intrinsic conductances. Because increases in $[Ca^{2+}]_i$ secondary to activation of NMDA receptor-mediated conductance are thought to be critical to the induction of synaptic plasticity in CA1

cells, the possible interaction between intrinsic ($g_{K(Ca)}$ and $g_{C(Ca)}$) and NMDA receptor-mediated conductances could have an important homeostatic function (Zorumski et al. 1989).

Implications of the modeling results

Numerical simulation provides an important means of testing hypotheses about neuronal signaling that cannot presently be settled experimentally. With the present model, our goal was to observe how the complex kinetics of NMDA receptor-mediated conductances might interact with intrinsic and synaptic conductances to produce short-term changes in the excitability of CA1 cells. The model was constructed with realistic physiological parameters (channel kinetics), but a relatively high level of anatomic abstraction, omitting fine (multiple dendritic branches) and microscopic (dendritic spine) structure. This matched the anatomic resolution of actual dendritic recordings in a previous study obtained at primary and secondary branches of the main dendrite (Poolos and Kocsis 1990b) and thus allowed fitting of model parameters to actual dendritic recordings.

The results indicate that by virtue of their voltage dependence and slow kinetics, NMDA receptor-mediated conductances are capable of generating substantial short-term response plasticity when synaptically activated in a train of stimuli. This response plasticity is evidenced as potentiation of the EPSP at dendritic and somatic sites, with increasing firing of action potentials at the soma, and also by substantial increases in $[Ca^{2+}]_i$ at the synaptic site. Activation of NMDA receptor-mediated conductances was sensitive to small changes in $[K^+]_o$ or in Ca^{2+}-sensitive K^+ conductances, demonstrating an interaction between synaptic and intrinsic conductances that is a consequence of the voltage-dependence of conduction through NMDA receptor-mediated channels. This also suggests that activity-dependent changes in $[K^+]_o$ or $[Ca^{2+}]_o$ might have a feedback effect on excitability.

The active properties of the dendritic arbor, although well established in the CA1 cell, were minimized in this model: only one compartment had Na^+ channels, and the density of g_{Ca} was decreased from estimates of that in CA3 cells (where Ca^{2+} spikes are more prominent). This reduced the nonlinearity of the dendritic membrane, substantially simplifying both interpretation and computation. It is likely however that local action potential generation would increase dendritic excitability by amplifying in time and spatial extent the depolarization produced by EPSPs. These effects have already been addressed at the level of the dendritic spine (Pongracz 1985; Shepherd et al. 1985) and may warrant further investigation. Such morphological details were not included in the present model; this issue is especially important in calculating the NMDA receptor-mediated $[Ca^{2+}]_i$ accumulation in spines in the context of long-term potentiation (LTP) of EPSPs (Holmes and Levy 1990).

Considering the preferred low-frequency transmission in passive dendrites, the NMDA-related slow potentials can reach a very large portion of the membrane surface facilitating heterosynaptic interaction. This “export” of primary synaptic activity can be further amplified by activating a spike-generating patch near the secondary input. Further analysis of this interaction between the slow NMDA-related depolarization and the spontaneous dendritic spike potentials should give insight into how the changes in the response of hippocampal neurons occur during repetitive synaptic activity.

Acknowledgements

This work was supported in part by the Medical Research Service at Department of Veterans Affairs, the National Institute of Neurological Disorders and Stroke Grant NS-06208, and the Office of Naval Research.

References

Alger BE, Nicoll RA. Feed-forward dendritic inhibition in rat hippocampal pyramidal cells studied in vitro. J Physiol Lond 1982;328:105–123. [PubMed: 7131309]

Allen GI, Eccles J, Nicoll RA, Oshima T, Rubia FJ. The ionic mechanisms concerned in generating the i.p.s.ps of hippocampal pyramidal cells. Proc R Soc Lond B Biol Sci 1977;198:363–384. [PubMed: 21396]

Ascher P, Nowak L. The role of divalent cations in the *N*-methyl-d-aspartate responses of mouse central neurones in culture. J Physiol Lond 1988;399:247–266. [PubMed: 2457089]

Bekkers JM, Stevens CF. Presynaptic mechanism for long-term potentiation in the hippocampus. Nature Lond 1990;346:724–729. [PubMed: 2167454]

Carnevale NT, Woolf TB, Shepherd GM. Neuron simulation with SABER. J Neurosci Methods 1990;33:135–148. [PubMed: 2232865]

Collingridge GL, Herron CE, Lester RAJ. Frequency-dependent *N*-methyl-d-aspartate receptor-mediated synaptic transmission in rat hippocampus. J Physiol Lond 1988;399:301–312. [PubMed: 2900333]

Collingridge GL, Kehl SJ, McLennan H. Excitatory amino acids in synaptic transmission in the Schaffer collateral-commissural pathway of the rat hippocampus. J Physiol Lond 1983;334:33–46. [PubMed: 6306230]

Davies CH, Davies SN, Collingridge GL. Paired-pulse depression of monosynaptic GABA-mediated inhibitory postsynaptic responses in rat hippocampus. J Physiol Lond 1990;424:513–531. [PubMed: 2167975]

Gamble E, Koch C. The dynamics of free calcium in dendritic spines in response to repetitive synaptic input. Science Wash DC 1987;236:1311–1315.

Gardner-Medwin AR. Analysis of potassium dynamics in mammalian brain tissue. J Physiol Lond 1983;335:393–426. [PubMed: 6875885]

Harris EW, Ganong AH, Cotman CW. Long-term potentiation in the hippocampus involves activation of *N*-methyl-d-aspartate receptors. Brain Res 1984;323:132–137. [PubMed: 6151863]

Herron CE, Lester RAJ, Coan EJ, Collingridge GL. Frequency-dependent involvement of NMDA receptors: a novel synaptic mechanism. Nature Lond 1986;322:265–268. [PubMed: 2874493]

Holmes WR, Levy WB. Insights into associative long-term potentiation from computational models of NMDA receptor-mediated calcium influx and intracellular calcium concentration changes. J Neurophysiol 1990;63:1148–1168. [PubMed: 2162921]

Jahr CE, Stevens CF. Glutamate activates multiple single channel conductances in hippocampal neurons. Nature Lond 1987;325:522–525. [PubMed: 2433593]

Jahr CE, Stevens CF. A quantitative description of NMDA receptor-channel kinetic behavior. J Neurosci 1990a;10:1830–1837. [PubMed: 1693952]

Jahr CE, Stevens CF. Voltage dependence of NMDA-activated macroscopic conductances predicted by single-channel kinetics. J Neurosci 1990b;10:3178–3182. [PubMed: 1697902]

Kocsis JD, Malenka RC, Waxman SG. Effects of extracellular potassium concentration on the excitability of the parallel fibers of the rat cerebellum. J Physiol Lond 1983;334:225–244. [PubMed: 6864558]

Konnerth A, Keller BU, Ballanyi K, Yaari Y. Voltage sensitivity of NMDA-receptor mediated postsynaptic currents. Exp Brain Res 1990;81:209–212. [PubMed: 2168319]

Larson J, Lynch G. Induction of synaptic potentiation in hippocampus by patterned stimulation involves two events. Science Wash DC 1986;232:985–988.

Llinas R, Sugimori M. Electrophysiological properties of in vitro Purkinje cell dendrites in mammalian cerebellar slices. J Physiol Lond 1980;305:197–213. [PubMed: 7441553]

Lynch G, Larson J, Kelso S, Barrioneuvo G, Schottler F. Intracellular injections of EGTA block induction of hippocampal long-term potentiation. Nature Lond 1983;305:719–721. [PubMed: 6415483]

Malinow R, Tsien RW. Presynaptic enhancement shown by whole-cell recordings of long-term potentiation in hippocampal slices. Nature Lond 1990;346:177–180. [PubMed: 2164158]

Masukawa LM, Prince DA. Synaptic control of excitability in isolated dendrites of hippocampal neurons. J Neurosci 1984;4:217–227. [PubMed: 6693938]

Mayer ML, Westbrook GL. Permeation and block of *N*-methyl-d-aspartic acid receptor channels by divalent cations in mouse cultured central neurones. J Physiol Lond 1987a;394:501–527. [PubMed: 2451020]

Mayer ML, Westbrook GL. The physiology of excitatory amino acids in the vertebrate nervous system. Prog Neurobiol 1987b;28:197–276. [PubMed: 2883706]

McCarren M, Alger BE. Use-dependent depression of IPSPs in rat hippocampal pyramidal cells in vitro. J Neurophysiol 1985;53:557–571. [PubMed: 2984352]

Miller JP, Rall W, Rinzel J. Synaptic amplification by active membrane in dendritic spines. Brain Res 1985;325:325–330. [PubMed: 2983830]

Nicoll RA, Kauer JA, Malenka RC. The current excitement in long-term potentiation. Neuron 1988;1:97–103. [PubMed: 2856092]

Nicoll RA, Malenka RC, Kauer JA. Functional comparison of neurotransmitter receptor subtypes in mammalian central nervous system. Physiol Rev 1990;70(2):513–565. [PubMed: 1690904]

Nowak L, Bregestovski PA, Ascher P, Herbet A, Prochiantz A. Magnesium gates glutamate-activated channels in mouse central neurones. Nature Lond 1984;307:462–465. [PubMed: 6320006]

Perkel DH, Perkel DJ. Dendritic spines: role of active membrane in modulating synaptic efficacy. Brain Res 1985;325:331–335. [PubMed: 2579708]

Pongrácz F. The function of dendritic spines: a theoretical study. Neuroscience 1985;15:933–946. [PubMed: 3900806]

Poolos NP, Kocsis JD. Elevated extracellular potassium concentration enhances synaptic activation of NMDA receptors in hippocampus. Brain Res 1990a;508:7–12. [PubMed: 2159824]

Poolos NP, Kocsis JD. Dendritic action potentials activated by NMDA receptor-mediated EPSPs in CA1 hippocampal pyramidal cells. Brain Res 1990b;524:342–346. [PubMed: 1981329]

Poolos NP, Mauk MD, Kocsis JD. Activity-evoked increases in extracellular potassium modulate presynaptic excitability in the CA1 region of the hippocampus. J Neurophysiol 1987;58:404–416. [PubMed: 3655875]

Rall, W. Handbook of Physiology. The Nervous System. 1. Washington, DC: Am Physiol Soc.; 1977. Core conductor theory and cable properties of neurons; p. 39-98.

Regehr WG, Tank DW. Postsynaptic NMDA receptor-mediated calcium accumulation in hippocampal CA1 pyramidal cell dendrites. Nature Lond 1990;345:807–810. [PubMed: 1972782]

Rutecki PA, Lebeda FJ, Johnston D. Epileptiform activity induced by changes in extracellular potassium in hippocampus. J Neurophysiol 1985;54:1363–1374. [PubMed: 2416891]

Saber User's Guide, Reference Manual, Guide to Writing Templates, MAST Reference Manual. Beaverton, OR: Analogy, Inc.; 1988.

Sah P, Hestrin S, Nicoll RA. Properties of excitatory postsynaptic currents recorded *in vitro* from rat hippocampal interneurones. J Physiol Lond 1990;430:605–616. [PubMed: 1982315]

Shepherd GM, Brayton RK. Logic operations are properties of computer-simulated interactions between excitable dendritic spines. Neuroscience 1987;21:151–165. [PubMed: 3601072]

Shepherd GM, Brayton RK, Miller JP, Segev I, Rinzel J, Rall W. Signal enhancement in distal cortical dendrites by means of interactions between active dendritic spines. Proc Natl Acad Sci USA 1985;82:2192–2195. [PubMed: 3856892]

Traub R. Simulation of intrinsic bursting in CA3 hippocampal neurons. Neuroscience 1982;7:1233–1242. [PubMed: 7110586]

Traub R, Llinas R. The spatial distribution of ionic conductances in normal and axotomized motorneurons. Neuroscience 1977;2:829–850.

Traub R, Llinas R. Hippocampal pyramidal cells: significance of dendritic ionic conductances in neuronal function and epileptogenesis. J Neurophysiol 1979;42:476–496. [PubMed: 422974]

Traub RD, Wong RKS, Miles R, Michelson H. A model of a CA3 hippocampal pyramidal neuron incorporating voltage-clamp data on intrinsic conductances. J Neurophysiol 1991;66:635–650. [PubMed: 1663538]

Traynelis SF, Dingledine R. Potassium-induced spontaneous electrographic seizures in the rat hippocampal slice. J Neurophysiol 1988;59:259–276. [PubMed: 3343603]

Turner DA, Schwartzkroin PA. Steady-state electrotonic analysis of intracellularly stained hippocampal neurons. J Neurophysiol 1980;44:184–199. [PubMed: 7420134]

Turner RW, Baimbridge KG, Miller JJ. Calcium-induced long-term potentiation in the hippocampus. Neuroscience 1982;7:1411–1416. [PubMed: 6126840]

Wickens J. Electrically coupled but chemically isolated synapses: dendritic spines and calcium in a rule for synaptic modification. Prog Neurobiol 1988;31:507–528. [PubMed: 2849143]

Wigstrom H, Gustafsson B. A possible correlate of the postsynaptic condition for long-lasting potentiation in the guinea pig hippocampus in vitro. Neurosci Lett 1984;44:327–332. [PubMed: 6145123]

Wigstrom H, Gustafsson B, Huang YY. A synaptic potential following single volleys in the hippocampal CA1 region possibly involved in the induction of long-lasting potentiation. Acta Physiol Scand 1985;124:475–478. [PubMed: 2864779]

Wong RK, Prince DA, Basbaum AI. Intradendritic recordings from hippocampal neurons. Proc Natl Acad Sci USA 1979;76:986–990. [PubMed: 284423]

Zucker RS. Short-term synaptic plasticity. Annu Rev Neurosci 1989;12:13–31. [PubMed: 2648947]

Zorumski CF, Thio LL, Clark GD, Clifford DB. Calcium influx through *N*-methyl-d-aspartate channels activates a potassium current in postnatal rat hippocampal neurons. Neurosci Lett 1989;99:293–299. [PubMed: 2542845]

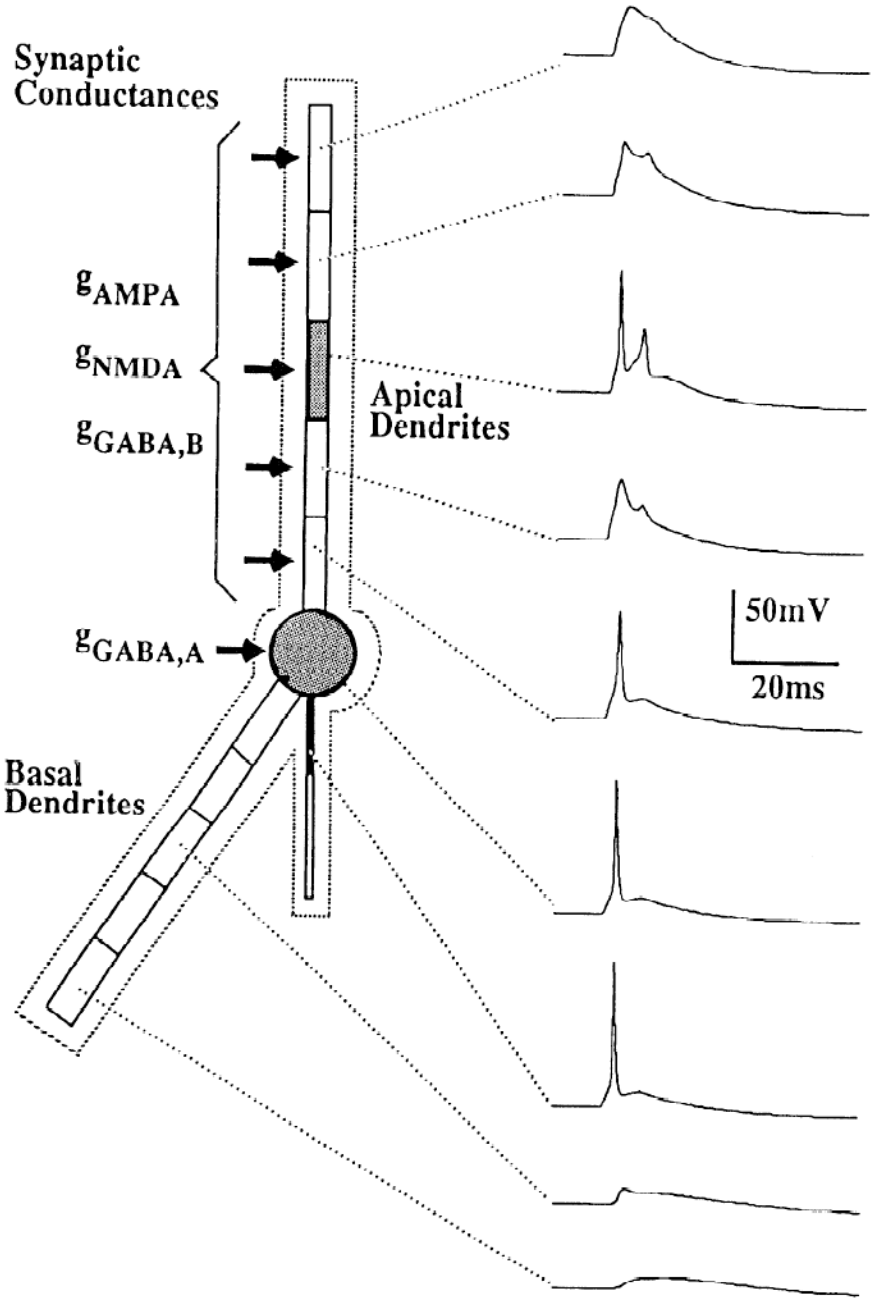

FIG. 1.

Schematic representation of the CA1 model with lumped apical and basal dendritic trees and extracellular K^+ layer for calculating the effects of extracellular K^+ concentration ($[K^+]_o$) accumulation. *N*-methyl-D-aspartate (NMDA), non-NMDA (AMPA), and γ-aminobutyric acid (GABA) receptor-mediated synaptic inputs are introduced into the apical compartments. The apical cylinder has 1 active compartment. On the *right* is shown the progressive development of the soma-dendritic response to a compound synaptic stimulus represented by arrows in the compartmental scheme. The following conductance values were applied for each synaptically stimulated compartment: $\bar{g}_{AMPA}$ = 50 nS, $\bar{g}_{NMDA}$ = 2 nS, $\bar{g}_{GABA,A}$ = 20 nS, and $\bar{g}_{GABA,B}$ = 10 nS.

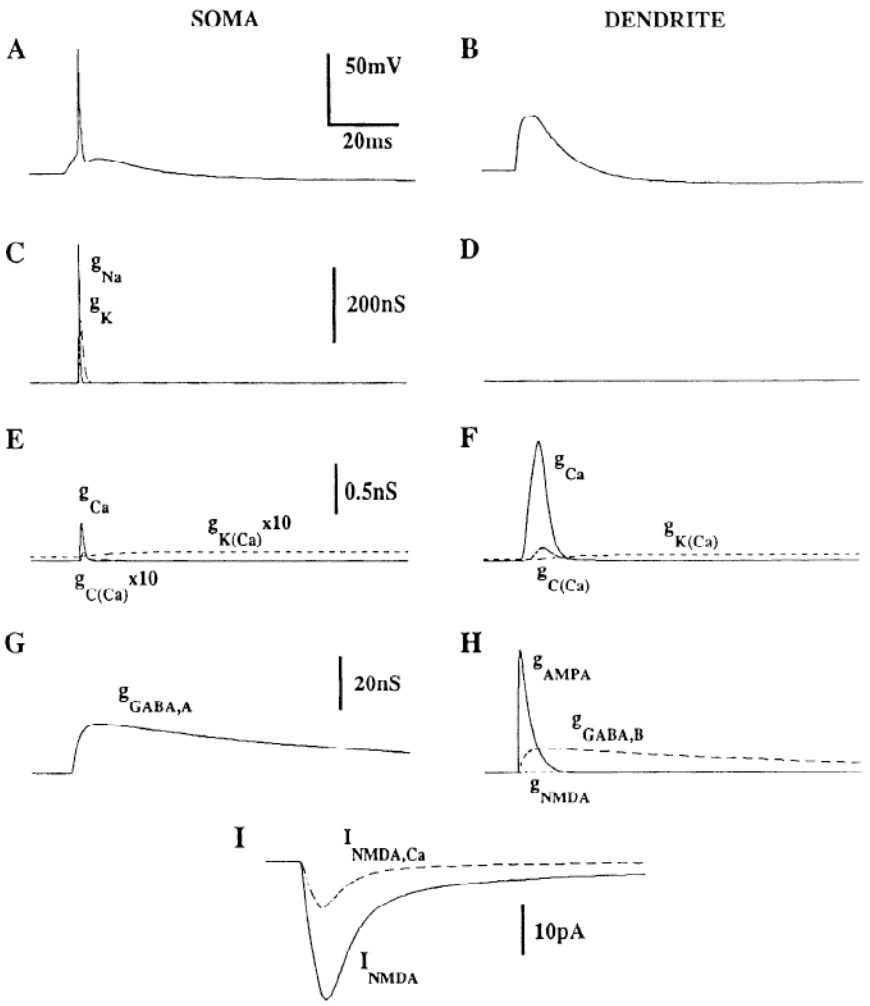

FIG. 2.

Synaptic conductances and voltage-dependent membrane conductances activated by a brief synaptic stimulus ($\bar{g}_S$ = 80 nS, $\bar{g}_{NMDA}$ = 2 nS, $\bar{g}_{AMPA,A}$ = 20 nS, and $\bar{g}_{AMPA,B}$ = 10 nS). *A* and *B*: voltage responses in the soma and the most distal compartment of the apical cylinder. *C–F*: conventional membrane conductances in the soma (*C* and *E*) and the dendrite (*D* and *F*). Note the differences between the somatic and dendritic g_{Ca} and $g_{C(Ca)}$ despite the same densities ($\bar{g}_{Ca}$, = 0.2 mS/cm^2 and $\bar{g}_{C(Ca)}$ = 1 mS/cm^2). *G* and *H*: different components of the synaptic stimulus: $GABA_A$ receptor-mediated inhibitory conductance in the soma (*G*); non-NMDA (AMPA) and NMDA receptor-mediated conductances and the $GABA_B$, receptor-mediated inhibitory conductance in the dendrite (*H*). *I*: total NMDA receptor-mediated synaptic current and its Ca^{2+} component flowing into 1 compartment of the apical cylinder. For abbreviations, see Fig. 1 legend.

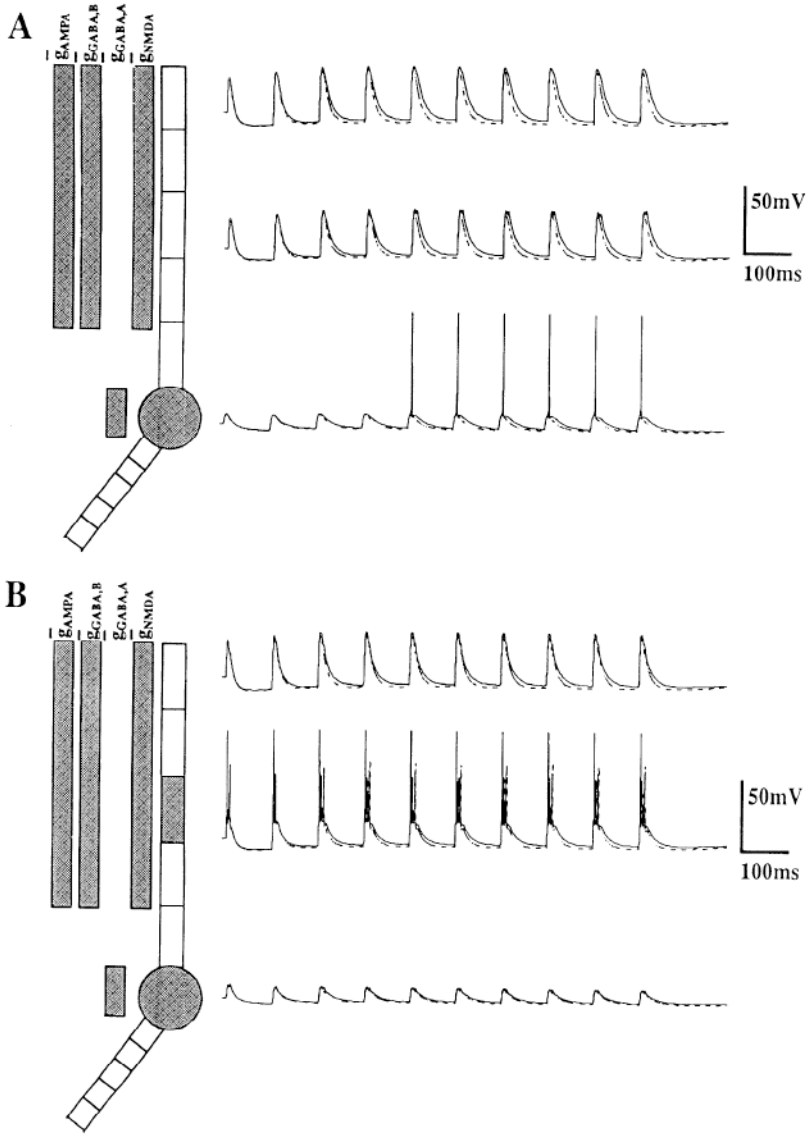

FIG. 3.

Effect of cumulative activation of NMDA receptor-mediated conductances during repetitive stimulation. *A*: comparison of the dendritic and somatic responses to a train of stimuli at 10 Hz during the activation of the NMDA receptor-mediated conductances ($\bar{g}_{NMDA}$ = 2 nS into each of 4 distal compartments of the apical tree: continuous curves) and the blockade of g_{NMDA} (*bottom curves* with interrupted lines). The other components of the synaptic input: $\bar{g}_{AMPA}$ = 40 nS, $\bar{g}_{GABA,B}$ = 10 nS (dendrite), and $\bar{g}_{GABA,A}$ = 20 nS (soma). The peak excitatory conductances during the first EPSP were 20% smaller according to experimental observations. *B*: similar curves as in *A*, but the apical cylinder contained 1 active compartment ($\bar{g}_{Na}$ = $\bar{g}_{K}$ = 10 mS/cm^2). Note the intensive spike activity in dendrites together with depression of somatic excitability. For abbreviations, see Fig. 1 legend.

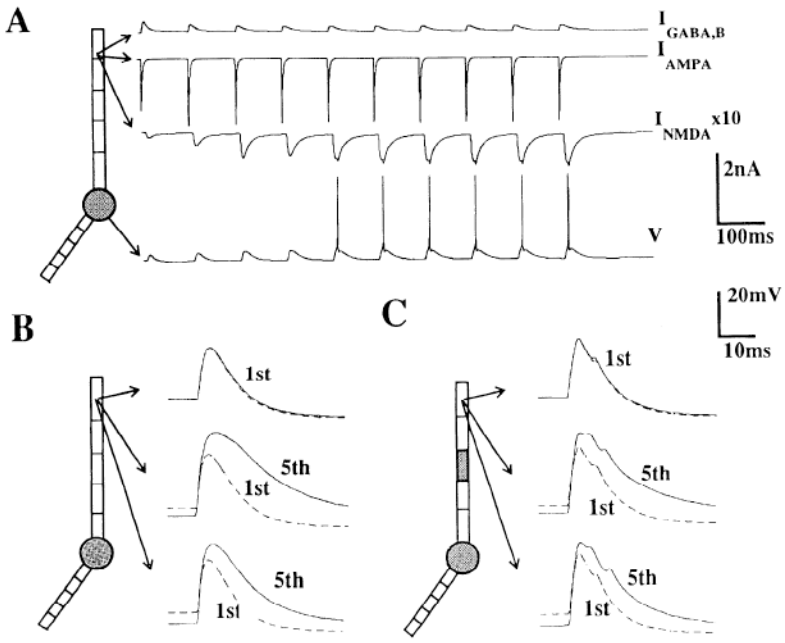

FIG. 4.

A: summary of synaptic currents activated during 10-Hz stimulation of the model cell. Note the progressive development of the *N*-methyl-D-aspartate (NMDA) receptor-mediated current. Peak values and distribution of synaptic conductances were the same as in Fig. 3. *Bottom trace*: somatic voltage record. *B* and *C*: simulated curves representing the effect of g_{NMDA} in the CA1 model neuron with inactive dendritic cylinders (*B*) and after addition of Na^+-K^+ conductances into the central dendritic compartment (*C*). In both groups of curves the *top curve* shows the first responses to a 10-Hz stimulation with g_{NMDA} present (continuous graph) and with blocked g_{NMDA} (interrupted graph). *Middle* and *bottom* curves compare the first and fifth responses with (*middle*) and without (*bottom*) g_{NMDA} representation.

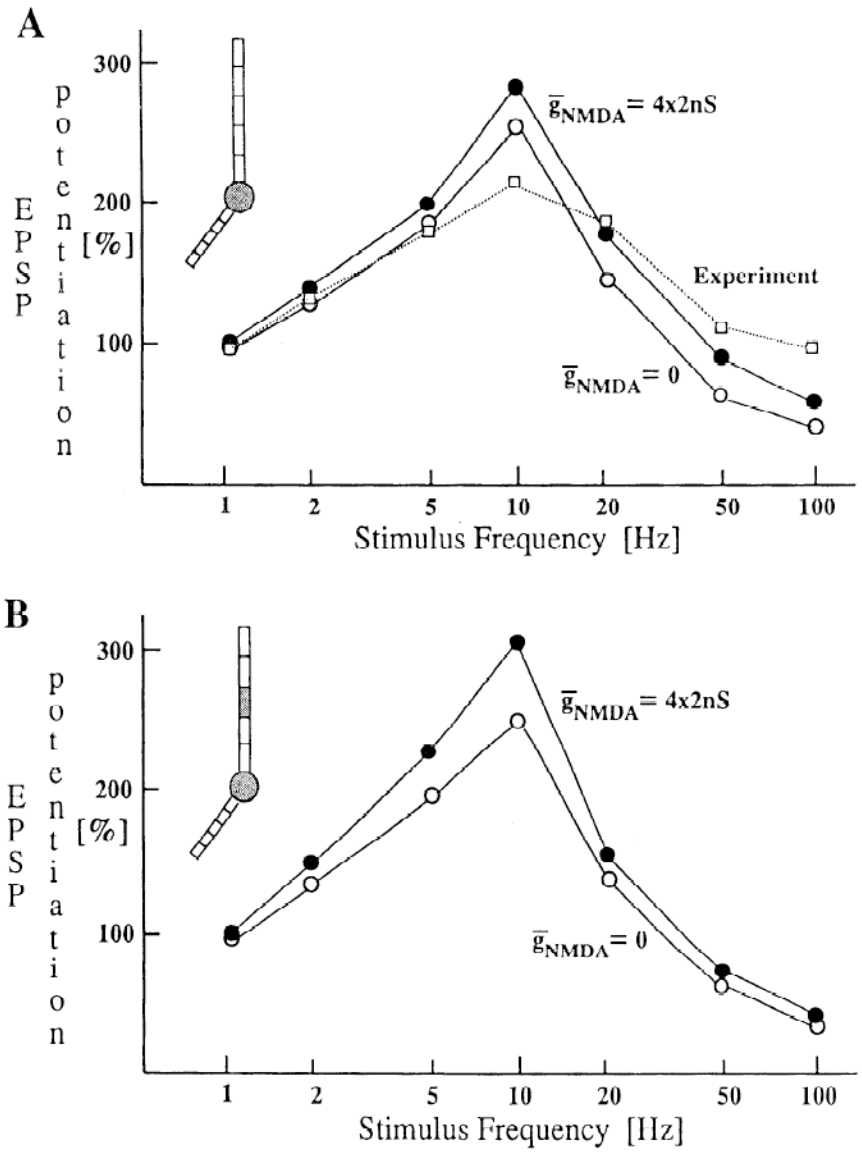

FIG. 5.

Diagrams characterizing the NMDA receptor-dependent potentiation of excitatory postsynaptic potentials (EPSPs) in the CA1 model. A: percent increase in the area bounded by the second EPSP in response to 2 successive stimuli presented at different frequencies. Responses remained subthreshold at each frequency ($\bar{g}_{NMDA}$ = 2 nS, $\bar{g}_{AMPA}$ = 20 Ns, $\bar{g}_{GABA,A}$ = 20 nS, and $\bar{g}_{GABA,B}$ = 10 nS with a distribution as in Fig. 3). The dotted diagram was calculated by means of experimental data. B: effects of activatin of dendritic spike generator on EPSP potentiatin in dendrites. The *bottom* curves in *A* and *B* represent EPSP potentiation with $\bar{g}_{NMDA}$ = 0. For abbreviations, see Fig. 1.

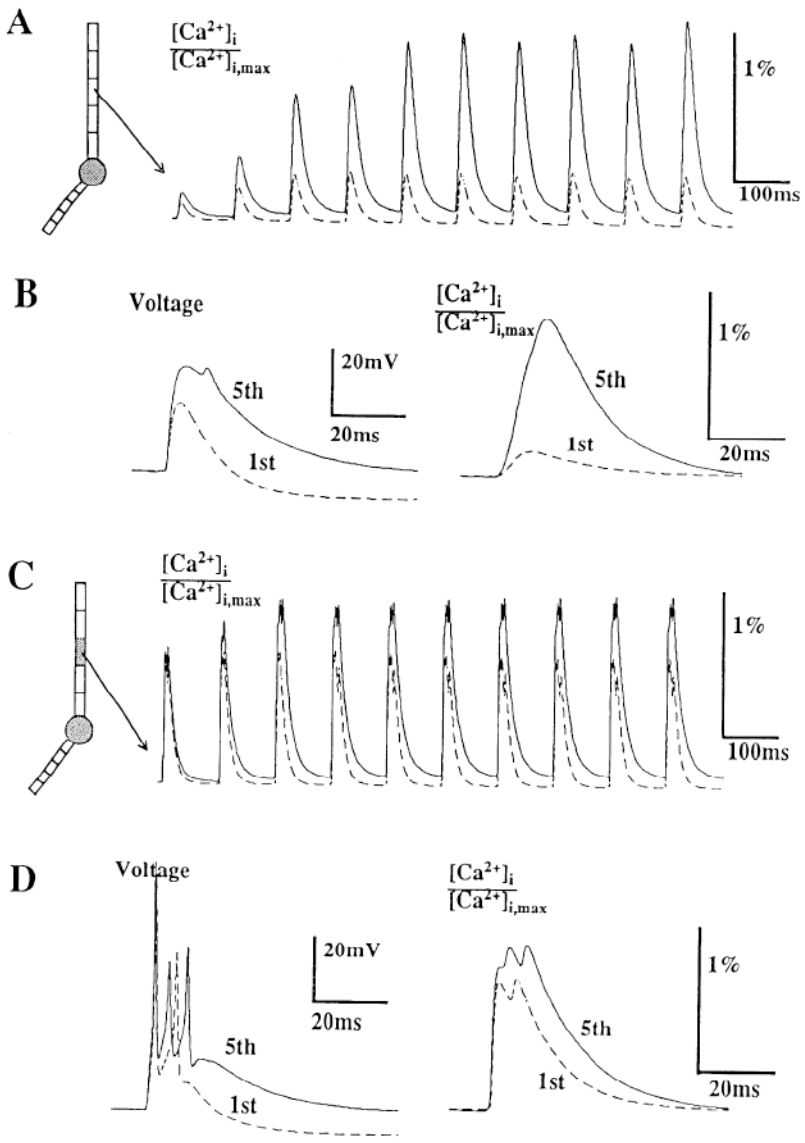

FIG. 6.

$[Ca^{2+}]_i$ accumulation induced by the *N*-methyl-D-aspartate (NMDA) receptor-mediated Ca^{2+} influx. *A*: intradendritic Ca^{2+} accumulation in the presence and absence of the NMDA receptor-mediated synaptic effects. The conventional Ca^{2+} conductance alone produced a much smaller $[Ca^{2+}]_i$ increase that changed little with an increase of g_{Ca} or the appearance of soma initial segment (IS) spikes (interrupted graph). In contrast, activation of g_{NMDA} elevated the intracellular Ca^{2+} into a much higher range (continuous graph). *B*: voltage responses and $[Ca^{2+}]_i$ transients (note the relative scale) at the synaptic site in the presence of the NMDA receptor-mediated conductance. The stimulation rate was 10 Hz; the first and fifth responses are superposed. *C* and *D*: same as in *A* and *B*, but the apical cylinder included 1 active compartment. Note the smaller difference of the amplitudes of the $[Ca^{2+}]_i$ during the activation of g_{NMDA} (continuous graph) and blockade of g_{NMDA} (interrupted graph). Intradendritic voltage and $[Ca^{2+}]_i$ signals at the first and fifth pulse expanded in time (g_{NMDA} active).

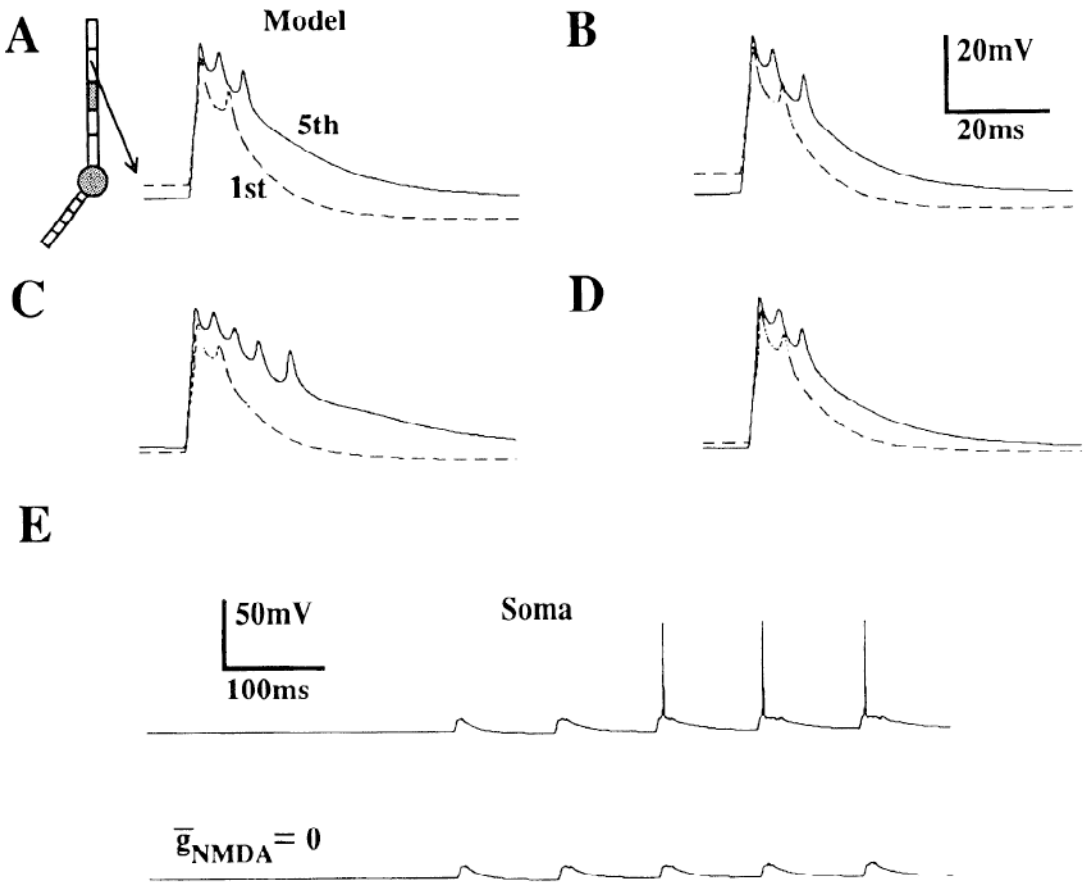

FIG. 7.

Elevated $[K^+]_o$ increased the excitability through an interaction with the NMDA receptor-mediated conductances. *A–D*: voltage responses to 10-Hz stimulation in the CA1 model incorporating 1 active dendritic compartment (5th response: continuous graph; 1st response: interrupted graph). *A*: pairs of responses under normal conditions. *B*: responses with NMDA conductances blocked showing diminished response potentiation. *C*: with $[K^+]_o$ at 5 mM, EPSP potentiation is increased compared with normal conditions. *D*: in elevated $[K^+]_o$ but with blocked NMDA conductances, EPSP potentiation is diminished to normal levels. *E*: somatic responses to repetitive stimulation in elevated $[K^+]_o$ showing somatic spiking with active NMDA conductances. For abbreviations, see Fig. 1 legend.

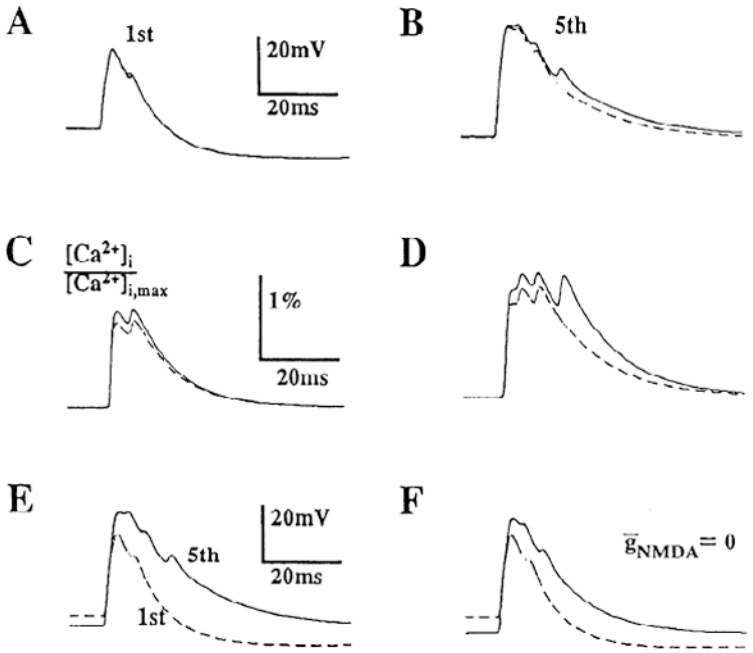

FIG. 8.

Effects of blocking $g_{K(Ca)}$ and $g_{C(Ca)}$ on NMDA receptor-mediated short-term potentiation. *A* and *B*: comparison of the intradendritic potentials in the model at the 1st (*A*) and 5th (*B*) stimulus in a 10-Hz train. The *top curves* were calculated with $\bar{g}_{K(ca)} = \bar{g}_{C(Ca)} = 0$. The apical cylinder had an active compartment similar to the previous figures. Note the increase in the number of small peaks on the falling phase of the fifth response (*B*). *C* and *D*: intracellular Ca^{2+} (on relative scale) at the synaptic site during the 1st (*C*) and 5th (*D*) stimulus. Blocking $g_{K(Ca)}$ and $g_{C(Ca)}$ produced a short term potentiation in the $[Ca^{2+}]_i$ (*top curves*). *E* and *F*: intradendritic potentials at the 1st (interrupted graph) and 5th (continuous graph) stimulus with $g_{K(Ca)} = g_{C(Ca)} = 0$. The blockade of g_{NMDA} decreased the EPSP potentiation later in the train (*F*: top curve). For abbreviations, see Fig. 1 legend.

TABLE 1

Geometric parameters and electrotonic lengths in the CA1 model

Structure	Length, μm	Diameter, μm	L	*n*	λ, μm
Apical dendrites	2725	5.8	0.8	5	3406
Basal dendrites	1859	4.8	0.6	5	3098
Soma	60	8.6	0.01	1	4147
IS	40	2	0.18	1	224
Axon trunk	500	1	5.75	1	87

L, lengths; *n*, number of compartments; IS, initial segment.

TABLE 2

Rate functions used in the CA1 model cell

Name	Rate Functions
g_{Na}	
α_m	$0.32(13 - V)/\{\exp[(13 - V)/4] - 1\}$
β_m	$0.28(V - 45)/\{\exp[V - 45)/5] - 1\}$
α_h	$0.128 \exp[(17 - V)/18]$
β_h	$4/(\exp[(40 - V)/5) + 1]$
g_K	
α_n	$0.032(15 - V)/\{\exp[(15 - V)/5] - 1\}$
β_n	$0.5 \exp[(10 - V)/40]$
g_{Ca}	
α_s	$1.6/\{1 + \exp[-0.072(V - 70)]\}$
β_s	$0.02(V - 51.1)/\{\exp[(V - 56.1)/5] - 1\}$
α_r	0.005 $[V \leq 0]$
	$\exp(-V/20)/200$ $[V > 0]$
β_r	0 $[V \leq 0]$
	$0.005\text{-}\alpha_r$ $[V > 0]$
$g_{K(Ca)}$	
α_q	$\min (0.00033[Ca^{2+}]_i/[Ca^{2+}]_{i,max}, 0.01)$
β_q	0.001
$g_{C(Ca)}$	
α_c	$\exp[(V - 10)/11 - (V - 6.5)/27]/19$ $[V \leq 50]$
	$2 \exp[-(V - 6.5)/27]$ $[V > 50]$
β_c	$2 \exp[-(V - 6.5)/27] - \alpha_c$ $[V \leq 50]$
	0 $[V > 50]$

TABLE 3

Membrane conductance densities and peak values of synaptic conductances in the soma, IS, and a single dendritic compartment

Name	Soma	Dendrite	IS
Membrane			
$\bar{g}_{Na}$, mS/cm^2	50	0–10	60
$\bar{g}_{K}$, mS/cm^2	50	0–10	40
$\bar{g}_{Ca}$, mS/cm^2	0.2	0.2	
$\bar{g}_{K(Ca)}$, mS/cm^2	1	1	
$\bar{g}_{C(Ca)}$, mS/cm^2	1	1	
Synapses			
$\bar{g}_{NMDA}$, nS		2	
$\bar{g}_{AMPA}$, nS		20–80	
$\bar{g}_{GABA,A}$, nS		20	
$\bar{g}_{GABA,B}$, nS		10	

For definition of variables, see text. IS, initial segment.